HHS Public Access

Author manuscript

Hepatology. Author manuscript; available in PMC 2017 February 01.

Published in final edited form as:

Hepatology. 2016 February ; 63(2): 550–565. doi:10.1002/hep.28024.

Jagged1 heterozygosity in mice results in a congenital cholangiopathy which is reversed by concomitant deletion of one copy of *Poglut1 (Rumi)*

Shakeel M. Thakurdas[1], **Mario F. Lopez**[1], **Shinako Kakuda**[2], **Rodrigo Fernandez-Valdivia**[3], **Neda Zarrin-Khameh**[4], **Robert S. Haltiwanger**[2], and **Hamed Jafar-Nejad**[1,5]

[1]Department of Molecular and Human Genetics, Baylor College of Medicine, Houston, TX.

[2]Department of Biochemistry and Cell Biology, Stony Brook University, Stony Brook, NY.

[3]Department of Pathology, School of Medicine, Wayne State University, Detroit, MI.

[4]Department of Pathology and Immunology, Baylor College of Medicine, Houston, TX.

[5]Program in Developmental Biology, Baylor College of Medicine, Houston, TX.

Abstract

Haploinsufficiency for the Notch ligand *JAG1* in humans results in an autosomal dominant, multisystem disorder known as Alagille syndrome, which is characterized by a congenital cholangiopathy of variable severity. Here we show that on a C57BL/6 background, jagged1 heterozygous mice ($Jag1^{+/-}$) exhibit impaired intrahepatic bile duct (IHBD) development, decreased SOX9 expression and thinning of the peri-portal vascular smooth muscle cell (VSMC) layer, which are apparent at embryonic day 18 and the first postnatal week. In contrast, mice double-heterozygous for *Jag1* and the glycosyltransferase *Poglut1* (*Rumi*) start showing a significant improvement in IHBD development and VSMC differentiation during the first week. At P30, $Jag1^{+/-}$ mice show widespread ductular reactions and ductopenia in their livers and a mild but statistically significant bilirubinemia. In contrast, P30 *Jag1/Rumi* double-heterozygous mice show well-developed portal triads around most portal veins, with no elevation of serum bilirubin. Conditional deletion of *Rumi* in VSMCs results in progressive arborization of the IHBD tree, whereas deletion of *Rumi* in hepatoblasts frequently results in an increase in the number of hepatic arteries without affecting bile duct formation. Nevertheless, removing one copy of *Rumi* from either VSMCs or hepatoblasts is sufficient to partially suppress the $Jag1^{+/-}$ bile duct defects. Finally, all Rumi target sites of the human JAG1 are efficiently glucosylated, and loss of *Rumi* in VSMCs results in increased levels of full-length JAG1 and a shorter fragment of JAG1 without affecting *Jag1* mRNA levels.

Conclusions—On a C57BL/6 background, *Jag1* haploinsufficiency results in bile duct paucity in mice. Removing one copy of *Rumi* suppresses the $Jag1^{+/-}$ bile duct phenotype, indicating that Rumi opposes the JAG1 function in the liver.

Contact Information, Corresponding author: Hamed Jafar-Nejad, Department of Molecular and Human Genetics, Baylor College of Medicine, One Baylor Plaza, Room 919E, Houston, TX 77030. hamedj@bcm.edu; Fax: 713-798-8142.

Keywords

Alagille syndrome; Notch signaling; Intrahepatic bile ducts; Vascular smooth muscle cells; Glycosylation

Introduction

The Notch signaling pathway is a vital component of many developmental processes in animals.[1] In mammals the pathway is composed of 4 receptors (Notch1-4) and 5 ligands (delta-like (DLL)1, 3, 4 and jagged (JAG)1, 2). The Notch pathway ligand JAG1 plays important developmental roles in a host of organ systems including IHBDs[2,3] and the cardiovascular system.[4] It is then no surprise that deleterious mutations in human *JAG1* result in an autosomal dominant, multisystem disease known as Alagille syndrome,[5–7] whose pathognomonic feature is a congenital cholangiopathy.[8] The cholangiopathy in Alagille syndrome is described as a decrease in the number of IHBDs or bile duct paucity, which is progressive at least in some patients.[8] The bile duct paucity can sometimes result in chronic cholestasis and liver cirrhosis,[9] for which no remedy is available except for liver transplantation.

The Notch signal transduction is quite straightforward and without second messengers.[10] Upon activation of the Notch receptor by its ligands, it undergoes several proteolytic cleavages, resulting in the release of the Notch intracellular domain (NICD) into the cytoplasm. The NICD is then translocated to the nucleus, where it functions as a transcriptional co-activator for CSL (CBF1, Suppressor of Hairless, Lag-1) transcription factors.[11] It then stands to reason that a significant number of posttranslational processes are devised during evolution to ensure tight regulation of the Notch pathway activation.[12] The extracellular domains of the Notch receptors contain 29–36 epidermal growth factor-like (EGF) repeats, which are the target of a number of posttranslational modifications, including glycosylation. Specifically, most Notch EGF repeats harbor consensus sequences for the addition of one or more *O*-linked glycans such as *O*-fucose, *O*-GlcNAc and *O*-glucose.[13] The enzyme responsible for the addition of *O*-glucose to EGF repeats is “protein *O*-glucosyltransferase 1” (POGLUT1) or Rumi, which was first discovered as an important regulator of Notch signaling in *Drosophila*.[14] However, due to the early lethality of *Rumi* mutant mouse embryos,[15] the role of mouse Rumi in the development of specific organ systems and regulation of specific Notch receptors and ligands is not known.

It has been reported that on a mixed genetic background, $Jag1^{+/-}$ heterozygous mice did not exhibit any defects in major organ systems other than eye abnormalities, and were born at Mendelian ratio.[16,17] Based on DBA staining of P0 liver sections on the progeny of a cross between $Rumi^{+/-}$ and $Jag1^{+/-}$ animals on a C57BL/6 background, we had previously concluded that removing one copy of *Rumi* results in the appearance of bile duct (BD) defects in *Jag1* heterozygous animals.[15] Here, we describe a detailed analysis of the bile duct development in several genetic models affecting *Jag1* and *Rumi* from embryonic day 18 to adulthood. Unexpectedly, we discovered a remarkable impairment in IHBD development associated with *Jag1* haploinsufficiency in mice. Moreover, we found that

contrary to our previous conclusion, reducing the gene dosage of *Rumi* gradually rescues the BD paucity in *Jag1*$^{+/-}$ livers, likely by altering the level of JAG1 protein. Conditional loss-of-function studies indicate that Rumi regulates the number of bile ducts and hepatic arteries around the portal veins (PV) in a JAG1-dependent manner. Our data offer insights into the potential mechanism by which the liver pathology in Alagille syndrome patients develops, and suggest that the balance between JAG1 and Rumi expression is required for the formation of normal portal triads.

Materials and Methods

Details are presented in the Supporting Materials.

Animal Breeding and Genotyping

All mice in this study were maintained on a C57BL/6J background. The *Jag1* deletion mutation (*Jag1*^{dDSL}) and the *Rumi* mutation (*Poglut1*$^{GT(IST10323G11)TIGM}$) have been described previously.[15,17] Mice heterozygous for *Jag1*^{dDSL} (abbreviated as *Jag1*$^{+/-}$) were backcrossed onto a C57BL/6J background for >10 generations for this study. For conditional deletion of *Rumi*, we used a previously described strategy[18] to generate a *Rumi*^{flox} allele containing loxP sites in introns 1 and 3 (Supporting Fig. S1). *Rumi*$^{flox/flox}$ animals are viable and fertile with no morphological abnormalities. *SM22α-Cre*[19] and *Albumin-Cre*[20] were obtained from Jackson Laboratory.

All mice were maintained in the pathogen-free barrier facility at Baylor College of Medicine and the studies were conducted in accordance with Animal Research Committee guidelines of the institute.

Antibodies

Immunohistochemistry: anti-mouse cytokeratin CK8, CK19 (DSHB, Iowa City, IA) both at 1:20 (an equal amount of anti-CK8 and anti-CK19 was combined and used at 1:20; referred throughout the study as ws-CK), anti-αSMA (1:200; Sigma, St. Louis, MO), anti-Ki67 (1:50; Cell Signaling Technologies, Danvers, MA), and anti-SOX9 (1:200; Millipore, Billerica, MA). Western blots: anti-Rumi (1:500),[15] anti-α-Tubulin (1:2000), anti-C-JAG1(C-20; 1:200), anti-N-JAG1 (H-66; 1:200) (Santa Cruz Biotechnology, Dallas, TX),.

Bile Duct and Hepatic Artery Quantification

Liver sections were taken from a similar depth and immunostained for biliary epithelial cells (BEC) with anti-cytokeratin antibodies. Portal triads in the entire section were counted and fully demarcated bile ducts with a visible lumen around each PV were recorded. These counts were then used to calculate the BD/PV ratio for each animal. For hepatic artery (HA) quantification, the same method was used to count vascular structures within the portal triad with a distinct surrounding layer of αSMA^{+} cuboidal cells and a clear lumen. These counts were then used to calculate the HA/PV ratio for each animal.

Resin Cast of the Biliary Tree

Resin casts were generated as reported previously with slight modifications,[21] and were imaged with a Leica Discovery V8 stereoscope and AxioCam MRc5 camera.

***O*-Glucose Site Mapping on Human JAG1—**Recombinant human JAG1-Fc with >90% purity (Adipogen, catalog # AG-40A-0081) was reduced and alkylated, separated by SDS-PAGE and subjected to in-gel protease digests as described previously.[22,23] Nano-LC-MS/MS was used to identify *O*-glucose modified glycopeptides based on neutral loss of the glycans during collision-induced dissociation as described.[24] Relative levels of the predicted glycoforms for each glycopeptide were analyzed using extracted ion chromatograms (EIC) for the appropriate parent ions as described previously.[24]

***Jag1* qRT-PCR Analysis—**Total RNA was extracted using TRI Reagent (Sigma) and Direct-zol RNA miniPrep kit (Zymo Research, Irvine, CA). qRT-PCR was performed using 100 ng total RNA per well and TaqMan One-Step RT-PCR Master Mix (Applied Biosystems). *Jag1* was detected using a commercially available assay (Applied Biosystems; Mm00496902_m1). Relative mRNA level was compared using the $2^{-\Delta\Delta CT}$ method, with 18S as control (4319413E, Applied Biosystems).

Statistical Analysis—Analysis of body weights, bile duct to portal vein and hepatic artery to portal vein ratios and serum TBR levels was carried out with two sample *t*-tests or one-way ANOVA. Progeny analysis was carried out using a chi-square test with three degrees of freedom.

Results

Jag1 Heterozygosity Results in Decreased Survival and a Mild Growth Retardation in Mice

Genotypic analysis of litters obtained from crosses between $Jag1^{+/-}$ and C57BL/6 (WT) mice at weaning time showed that only 34% of the progeny are $Jag1^{+/-}$. This is significantly less than the expected Mendelian ratio of 50% (Table 1) and is in agreement with a previous report[25]. We genotyped a few litters at P0–P7 and found a similar difference in birth ratio between $Jag1^{+/-}$ and WT pups ($Jag1^{+/-}$ = 9 vs. WT = 17). Moreover, we genotyped a few stillborn pups retained from these crosses and found all of them to be $Jag1^{+/-}$. Together, these results indicate that some $Jag1^{+/-}$ mice die in the perinatal or late embryonic period.

To examine whether loss of one copy of *Rumi* modifies this phenotype, we performed a similar analysis on progeny from $Jag1^{+/-} \times Rumi^{+/-}$ crosses. Rather surprisingly, we found that at P30, the *Jag1/Rumi* double heterozygous ($J1R^{+/-}$) animals showed a trend towards better survival compared to their $Jag1^{+/-}$ littermates, which were still significantly less than the expected Mendelian ratio (Table 1). A comparison of the body weights of these P30 mice revealed a similar pattern among the four genotypes, with $Jag1^{+/-}$ mice showing a statistically significant growth retardation compared to WT littermates, and $J1R^{+/-}$ littermates trending towards WT body weight levels (Table 1). These observations suggest that decreasing the level of Rumi partially suppresses the peri/neonatal lethality of $Jag1^{+/-}$ animals and improves their growth.

Severe Bile Duct Paucity in *Jag1*$^{+/-}$ Mice during the First Postnatal Week and Its Improvement by Loss of One Copy of *Rumi*

To examine the effects of decreasing the gene dosage of *Jag1*, *Rumi* or both on IHBD development, livers from P0, P3 and P7 progeny of *Jag1*$^{+/-}$ × *Rumi*$^{+/-}$ crosses were analyzed by immunostaining with antibodies against cytokeratins (CK8 & CK19, hereafter called ws-CK) and SOX9 for BECs, and αSMA for VSMCs. Whereas WT and *Rumi*$^{+/-}$ mice start forming well-demarcated, lumenized and symmetrically staining BDs at P0 (Fig. 1A,A',D,D'), *Jag1*$^{+/-}$ littermates at this age show a paucity of such structures in the hilar PVs and complete absence in the peripheral PVs (Fig. 1B,B'). This was associated with a generally weak SOX9 expression in *Jag1*$^{+/-}$ BECs, and fewer CK-positive BECs around *Jag1*$^{+/-}$ PVs compared to WT littermates, until P3 and especially at P0 (Fig. 1B,B',F,F' compare to 1A,A',E,E'). Even though SOX9 and CK-positive BECs start appearing in abundance around PVs of *Jag1*$^{+/-}$ mice by P7, there is still a severe paucity of patent bile ducts in these livers (Fig. 1J,J' compare to 1I,I'). These observations indicate that on a B6 background, IHBD development in mice is also sensitive to *Jag1* dosage as in humans and that *Jag1* haploinsufficiency in mice does in fact result in a congenital cholangiopathy.

Although not so obvious at P0 (Fig. 1C,C'), by P3 (Fig. 1G,G') and particularly at P7 (Fig. 1K,K') *J1R*$^{+/-}$ animals start showing a noticeable improvement in IHBD morphology and numbers compared to *Jag1*$^{+/-}$ littermates. Most notable is the frequent appearance of patent bile ducts in the peripheral PVs of *J1R*$^{+/-}$ livers (Fig. 1K'), something which was not observed in any of the seven *Jag1*$^{+/-}$ livers we analyzed at this time point (1J'). Quantification of the number of BDs associated with PV branches at P3 and P7 revealed a severe decrease in the BD/PV ratio in *Jag1*$^{+/-}$ compared to WT and *Rumi*$^{+/-}$ livers (Fig. 1M). Of note, although the BD/PV ratio for WT, *Jag1*$^{+/-}$ and *Rumi*$^{+/-}$ livers remained almost the same at these two time points, *J1R*$^{+/-}$ livers showed a gradual increase in the BD/PV ratio, from 0.48 at P3 to 0.60 at P7 (Supporting Fig. S2A,B). These observations indicate that decreasing the level of Rumi in a *Jag1* deficient mouse improves the IHBD developmental defects seen in *Jag1*$^{+/-}$ livers.

Reducing the Gene Dosage of *Rumi* Enhances BEC and VSMC recruitment around Embryonic Portal Veins in *Jag1*$^{+/-}$ mice

To further understand the biliary developmental processes that are affected by a decrease in JAG1 and Rumi, we examined embryonic livers of E18 litters from *Jag1*$^{+/-}$ × *Rumi*$^{+/-}$ crosses. In agreement with our observations at P0 and P3, we found that SOX9 expressing cells around E18 *Jag1*$^{+/-}$ PVs were markedly reduced compared to their WT and *Rumi*$^{+/-}$ littermates (Fig. 2B2, compare to 2A2,D2; 2E). However, removing one copy of *Rumi* in a *Jag1*$^{+/-}$ background significantly increased the number of SOX9^{+} cells around *J1R*$^{+/-}$ portal tracts (Fig. 2C2, compare to 2B2; 2E). Correspondingly, the ductal plates around *Jag1*$^{+/-}$ PVs appear sparse and less organized than all the other genotypic littermates, as indicated by ws-CK staining (Fig. 2B1, compare to 2A1,C1,D1). Furthermore, we observed a generally narrower αSMA expression domain around *Jag1*$^{+/-}$ PVs than their counterparts (Fig. 2B3, compare to 2A3,C3,D3). This is not surprising given the important role played by vascular endothelial JAG1 in the differentiation of VSMCs[4]. Taken together, these data indicate that

both BEC specification and portal mesenchyme development are impaired in *Jag1*$^{+/-}$ animals as early as E18.

Removing One Copy of *Rumi* in *Jag1*$^{+/-}$ Mice Alleviates the Liver Abnormalities Associated with *Jag1* Haploinsufficiency by One Month of Life

Examination of livers from one-month-old mice shows that loss of one copy of *Jag1* results in a variably expressed phenotype consistent with the variable presentation of Alagille syndrome in humans, even among patients who have the same *JAG1* mutation.[6,8] In its severe form (five out of 11 livers examined at this age), P30 *Jag1*$^{+/-}$ livers were peppered with focal necroinflammatory lesions throughout the liver, with biliary-type ductular reactions[26] surrounding up to 70% of portal veins (Fig. 3B,F,J,J',M compare to 3A,E,I,I',D,H,L,L'. See also Supporting Fig. S3). Ductular reactions, especially in the liver periphery, were observed in ~80% (9/11) of all livers analyzed at P30, together with ductopenia in the non-reactive PVs, which was observed in all 11 livers examined (data not shown). Because of this variability, we compared livers from *J1R*$^{+/-}$ mice only with *Jag1*$^{+/-}$ livers from the same litter. We found that in every litter obtained from the *Jag1*$^{+/-}$ × *Rumi*$^{+/-}$ cross, the *J1R*$^{+/-}$ liver (n = 6) was either normal or showed much milder phenotypes compared to its *Jag1*$^{+/-}$ siblings (Fig. 3C,G,K,K' compare to 3B,F,J,J'). Indeed, complete portal triads containing a PV, BDs, and hepatic arteries (HA) were readily observed in the majority of liver sections from P30 *J1R*$^{+/-}$ animals (Fig. 3K,K'). Also noticeable at this stage is the frequent thickening of peri-portal mesenchyme seen in *Rumi*$^{+/-}$ livers, especially around the BDs, and more prominent αSMA staining of HA walls in some arteries (Fig. 3L, L'). Consistent with these observations, P30 *Jag1*$^{+/-}$ mice exhibit a small but statistically significant increase in the level of serum total bilirubin (TBR) compared to their WT, *Rumi*$^{+/-}$ and *J1R*$^{+/-}$ littermates (Fig. 3N). Together, these observations provide further evidence that reducing the gene dosage of *Rumi* enhances the function of JAG1 in the liver.

Loss of *Rumi* in the Peri-Portal Mesenchyme Results in Progressive Arborization of the IHBDs

Given that *Rumi*$^{-/-}$ embryos die in mid-gestation,[15] we used the Cre-loxP approach[27] to determine the role of Rumi in bile duct development. We performed targeted deletion of *Rumi* in the peri-portal mesenchyme using *SM22α-Cre*[19] and in hepatoblasts and their progeny (hepatocytes and BECs) using *Albumin-Cre*.[20] Analysis of *Albumin-Cre*; *Rumi*$^{flox/flox}$ (*Rumi*^{AlbKO}) livers at P7, P42 and 5 months revealed no remarkable difference in IHBD development between WT and *Rumi*^{AlbKO} livers (Fig. 4B,D,F,H compare to A,D,E,G), although PCR and Western blot analyses indicate specific deletion of *Rumi* in the liver (Supporting Fig. S1). Instead, we noticed well-formed HAs with strong αSMA expression in the portal tracts (PT) of *Rumi*^{AlbKO} P7 livers even in the liver periphery (Fig. 4B, arrow), something we never observed in any P7 WT livers or the other genotypes studied at P7 (Fig. 4A,C, also see Fig. 1). The HA/PV ratio was significantly increased in *Rumi*^{AlbKO} P7 livers compared to control livers (Supporting Fig. S4A). In line with this unexpected finding, adult *Rumi*^{AlbKO} livers exhibited an increase in the number of HAs in their PTs, usually in close proximity to BDs (Fig. 4F,H compare to 4E,G; See Supporting Fig. S4B for HA quantification at 5 months). These observations suggest that expression of

Rumi in hepatoblast lineage is not essential for IHBD formation but is involved in the regulation of HA development.

SM22α-Cre; *Rumi*$^{flox/flox}$ (*Rumi*^{SMKO}) livers show a modest but statistically significant increase in the number of BDs per PV at P7 (Fig. 4C,D), frequently accompanied by stronger and thicker αSMA staining in the portal mesenchyme compared to control livers (Fig. 4C compare to 4A). In P42 liver sections as well, a larger number of patent BDs can be observed around PVs of *Rumi*^{SMKO} livers compared to WT littermates (Fig. 4I–K). These observations compelled us to employ a 3D resin-casting technique to properly visualize the changes suggested by immunohistological data. Interestingly, 3D resin casts of 4 month old intrahepatic biliary trees show the difference much more prominently with a highly arborized intrahepatic biliary tree in *Rumi*^{SMKO} livers compared to WT (Fig. 4M,M' compare to 4L,L'). Together, these data indicate that loss of Rumi in VSMCs results in an increase in the number of bile ducts in the mouse liver.

The increase in the number of BD per PV in *Rumi*^{SMKO} livers can be due to increased BEC specification, BEC proliferation, enhanced remodeling of the available BECs into patent bile ducts, or a combination of these mechanisms. To determine the potential mechanism(s) for this phenotype, we stained *Rumi*^{SMKO} and control livers at several time points with antibodies against the BEC markers SOX9 and wsCK and the proliferation marker Ki67. We did not observe an increase in the number of SOX9^{+} cells per portal vein in P0 or P7 *Rumi*^{SMKO} mice compared to their WT siblings (Fig. 4N–P). Moreover, there was no significant difference in the number of proliferating CK^{+} cells between WT and *Rumi*^{SMKO} livers at P7 (Fig. 5A–C). Together, these observations suggest that the increased number of BDs in P7 *Rumi*^{SMKO} livers is not primarily due to excessive BEC specification or BEC proliferation, and is likely because of enhanced remodeling of BECs into bile ducts, in agreement with the important role that JAG1 from VSMCs plays in this process.[3]

In contrast to P7 *Rumi*^{SMKO} livers, the increase in BDs observed in P42 *Rumi*^{SMKO} livers is accompanied by a small but significant increase in the number of SOX9-expressing cells around the PVs, especially those further away from the hilum (Fig. 4P and Supporting Fig. S4C). In addition, we observed significantly more proliferating BECs in P42 *Rumi*^{SMKO} livers compared to their WT littermates, especially in the peripheral portal tracts (Fig. 5D–F). These data suggest that BEC proliferation contributes to the increased DB/PV ratio observed in adult *Rumi*^{SMKO} livers.

Removing One Copy of *Rumi* either in the Hepatoblast or Smooth Muscle Compartment Alleviates the *Jag1*$^{+/-}$ Phenotype

We next examined whether reducing the gene dosage of *Rumi* in the hepatoblast or smooth muscle compartment is sufficient to reverse the *Jag1*$^{+/-}$ associated biliary abnormalities. To this end, we generated *Jag1*$^{+/-}$; *Albumin-Cre*; *Rumi*$^{flox/+}$ (*J1*$^{+/-}$*R*$^{Alb+/-}$) and *Jag1*$^{+/-}$; *SM22α-Cre*; *Rumi*$^{flox/+}$ (*J1*$^{+/-}$*R*$^{SM+/-}$) animals and compared their livers to those of their siblings. Examination of livers at P30 revealed better IHBD development in both *J1*$^{+/-}$*R*$^{Alb+/-}$ and *J1*$^{+/-}$*R*$^{SM+/-}$ mice compared to their *Jag1*$^{+/-}$ littermates (Fig. 6A–G). It is noteworthy that normal portal triads were observed more frequently in *J1*$^{+/-}$*R*$^{Alb+/-}$ livers compared to *J1*$^{+/-}$*R*$^{SM+/-}$ livers (Fig. 6E',F' and G). In agreement with these observations, removing one

copy of *Rumi* with each Cre line decreased the serum TBR levels in P30 *Jag1*$^{+/-}$ animals (Fig. 6H). Together, these data indicate that removing one copy of *Rumi* from either hepatoblasts or the VSMCs can partially compensate for the *Jag1* haploinsufficiency.

αSMA staining of the P30 liver sections from animals lacking one copy of *Rumi* with either Cre line also showed an increase in the number of HA branches per PV, although the difference between control and *Rumi*$^{AlbKO/+}$ livers did not reach statistical significance (Fig. 6B–C', and G). Importantly, simultaneous loss of one copy of *Jag1* decreased the intensity of αSMA staining and the number of peri-portal HAs in *Rumi*$^{SMKO/+}$ and to a lesser extent in *Rumi*$^{AlbKO/+}$ livers (Fig. 6E,E',F,F', and G). Of note, almost every *Jag1*$^{+/-}$ liver we have examined to date showed a dearth of HAs in the portal tracts (Fig. 6D,D', and G). Together, these data suggest that JAG1 from Albumin-Cre^{+} and SM22α-Cre^{+} lineages plays a role in arterial development in the portal tracts, and that Rumi negatively regulates this function of JAG1.

Deletion of *Rumi* in VSMCs Alters JAG1 Protein Level in These Cells

Our genetic experiments indicate that reducing Rumi levels promotes the function of JAG1 in the liver. Accordingly, we decided to examine whether loss of Rumi affects the level of JAG1 in mouse cells. To this end, we harvested and cultured VSMCs from the inferior vena cavae of 6-week old WT and *Rumi*^{SMKO} mice and performed Western blot on cell lysates prepared from confluent cultures. As shown in Fig. 7A, Rumi (~46 kDa) was completely absent in *Rumi*^{SMKO} VSMCs, confirming that our conditional allele deletes *Rumi* upon Cre expression. When probed with an antibody that binds to the C-terminal region of JAG1 (C-JAG1), we observed an increase in the level of full-length JAG1 (JAG1-FL) in *Rumi*^{SMKO} VSMCs (Fig. 7B,C; "Band 1"). Moreover, a ~50 kDa fragment in the lysates was also raised in *Rumi*^{SMKO} cells (Fig. 7B,C; "Band 3"). qRT-PCR assay on RNA harvested from VSMC cultures at the same time as protein harvest showed no difference in *Jag1* mRNA levels between WT and *Rumi*^{SMKO} VSMCs (Fig. 7D). As a type I transmembrane protein, the C-terminal part of JAG1 resides inside the cell (Fig. 7F). Therefore, we predicted that a soluble fragment of JAG1 corresponding to the 50 kDa band in Fig. 7B should be detectable in the media, at least in that conditioned by *Rumi*^{SMKO} cells. To test this, we analyzed media conditioned by WT or *Rumi*^{SMKO} VSMCs with an antibody against the N-terminal region of JAG1 (N-JAG1). Indeed, upon culturing ~10,000 VSMCs from each genotype, we detected a ~70 kDa fragment in the *Rumi*^{SMKO} culture medium but not in the control medium (Fig. 7E). Together, these data suggest that loss of Rumi increases the level of JAG1 protein in VSMCs and the level of a soluble extracellular fragment of JAG1 secreted by these cells.

JAG1 is Efficiently O-glucosylated on All Four Predicted Sites

Mouse and Human JAG1 harbor four consensus sequences for *O*-glucosylation by Rumi in the same EGF repeats[15,28] (Fig. 7F). However, the presence of *O*-glucose on JAG1 has not been verified experimentally. To address this issue, we performed mass spectrometric analysis on human JAG1 extracellular domain and analyzed the relative levels of naked (unglycosylated) and glycosylated forms of each peptide by using extracted ion chromatograms (EIC).[24] The data shown in Fig. 7G indicate that all four predicted Rumi target sites are efficiently *O*-glucosylated, as the trace corresponding to the naked peptides

(black line in Fig. 7G) was either a minor component of the EIC data (EGF4 and EGF16) or was not detected at all (EGF8 and EGF11). These observations indicate that JAG1 is a bona fide target for *O*-glucosylation by Rumi and suggest that the negative effect of Rumi on the function of JAG1 might be direct.

Discussion

The phenotypes of Alagille syndrome patients with *JAG1* deletion are very similar to those observed in patients with missense mutations, indicating that haploinsufficiency for *JAG1* causes Alagille syndrome.[29,30] However, previous studies did not report a liver phenotype in *Jag1*$^{+/-}$ mice.[16,17] In our current study, using *Jag1*$^{+/-}$ mice on a B6 background, we describe an impairment in bile duct morphogenesis which can be appreciated as early as day 18 of mouse gestation. These defects lead to bile duct paucity in the developing liver accompanied by ductular reactions, possibly to compensate for the deficiency. In spite of the bile duct paucity seen in *Jag1*$^{+/-}$ mice at P7, we did not observe overt jaundice in any of the mice studied. This discrepancy between mouse and human outcomes of *Jag1* haploinsufficiency in liver could be explained by a more efficient compensatory mechanism in mice, or simply the controlled environment and monotonous diet that experimental mice are bred under. Our data indicate that *Jag1*$^{+/-}$ mice on a B6 background can be used as a model to study the molecular mechanisms of bile duct abnormalities caused by *Jag1* haploinsufficiency and the compensatory mechanisms of the liver in this context. *Jag1*$^{+/-}$ livers show a severe decrease in SOX9 expression and an apparent reduction in BEC and VSMC recruitment during perinatal development. Previous reports indicate that loss of SOX9 results in a delay in biliary morphogenesis and provide strong evidence that SOX9 is a direct target of Notch signaling in the liver.[31,32] Moreover, expression of JAG1 in VSMCs is required for normal bile duct morphogenesis.[3] Therefore, decreased SOX9 expression and impaired differentiation and/or recruitment of the peri-portal VSMSs likely contribute to the *Jag1* haploinsufficient phenotype in the liver.

Genetic experiments with *Jag1*$^{+/-}$ animals allowed us to identify a dominant suppressor of the *Jag1*$^{+/-}$ liver phenotypes, namely *Poglut1* (*Rumi*), which encodes the only known enzyme in animals capable of adding *O*-linked glucose to EGF repeats.[14,15,33] Mutations in fly *rumi* result in a temperature-sensitive loss of Notch signaling in all contexts examined so far,[14,34,35] indicating that *O*-glucose promotes Notch signaling in *Drosophila*.[14,34] Transgenic expression of human Rumi can rescue the loss of Notch signaling in fly *rumi* mutants,[33] and RNAi-mediated knock-down of Rumi in several mammalian cell lines impairs Notch target gene expression and Notch1 cleavage.[15,36] Together, these observations suggested that the function of Rumi is fully conserved between flies and mammals, i.e., Rumi promotes Notch signaling in all contexts. However, our current data indicate that this is not the case. First, although conditional loss of *Notch2* with *Albumin-Cre* severely impairs IHBD development,[37] *Rumi*^{AlbKO} animals do not show bile duct morphogenesis defects, suggesting that *O*-glucosylation is not essential for the function of Notch2 in hepatoblasts. Second, removing one copy of *Rumi* in *Jag1*$^{+/-}$ animals improves SOX9 expression, bile duct formation, VSMC differentiation and serum bilirubin levels. Finally, *Rumi*^{SMKO} animals show an increase in the number bile ducts, but *Jag1*^{SMKO} animals show a decrease in the number of bile ducts.[3] Together, these observations indicate

that wild-type levels of Rumi negatively regulate JAG1-mediated Notch signaling in the liver.

Fly Notch and mammalian Notch1 and Notch2 have a large number of Rumi target sites (17–18) that are efficiently *O*-glucosylated by Rumi, indicating that presence of a Rumi target site is highly predictive for *O*-glucosylation.[14,15,24,38] However, while the fly homolog of JAG1 (Serrate) does not contain any *O*-glucose sites, mouse and human JAG1 proteins have four Rumi target sites (Figure 7F).[15,28] Our mass spectrometric analysis indicates that these four sites are efficiently glucosylated. Moreover, VSMCs isolated from *Rumi*^{SMKO} animals show an increase in the level of cellular JAG1 and also a soluble form of JAG1 in the medium without exhibiting an increase in the level of *Jag1* mRNA. Together, these data support the inference that Rumi directly regulates the function of JAG1 by post-translational modification of its extracellular domain. Soluble forms of JAG1 can activate or inhibit Notch signaling depending on expression level, the status of the soluble JAG1 as monomeric versus multimeric, and the cellular context.[39,40] Therefore, the increase in the level of full-length and/or soluble JAG1 might underlie the improvement of the *Jag1*$^{+/-}$ liver phenotypes upon decreasing *Rumi* gene dosage. Of note, our data indicate that the xylose-xylose-glucose-*O* trisaccharide is the predominant glycoform found on JAG1 EGF repeats, similar to the *O*-glucose glycans on the mammalian Notch1 and Notch2 (S.K. and R.S.H., unpublished data).[15,24] Given our recent report on the negative regulation of the Notch receptor activity by xylose residues,[41] it is also possible that the negative effect of *O*-glucose glycans on JAG1-induced signaling is mediated by the xylose residues present in the trisaccharides on JAG1 and/or Notch receptors.

A surprising aspect of *Rumi* phenotypes in the liver is the dramatic increase in the number of hepatic arteries in *Rumi*^{AlbKO} animals. It has been proposed that during normal liver development, hepatoblasts, cholangiocytes and/or hepatocytes secrete factors like vascular endothelial growth factor (VEGF) and Angiopoietin-1, which cooperate to induce hepatic artery formation in the vicinity of biliary structures and to recruit VSMCs to the hepatic arterial wall.[42] VEGF and Angiopoietin-1 do not contain EGF repeats,[43,44] and this makes them very unlikely targets for Rumi, as Rumi only adds *O*-glucose to properly folded EGF repeats.[45] However, JAG1 functions as a pro-angiogenic factor in several contexts,[46,47] and is required for vascular smooth muscle development.[4] These reports, combined with the weak αSMA staining around hepatic arteries in *Jag1*$^{+/-}$ animals and the suppression of the increase in the number of hepatic arteries observed in *Rumi*$^{AlbKO/+}$ and *Rumi*$^{SMKO/+}$ livers upon removing one copy of *Jag1* suggest that JAG1 in these cell types is involved in arterial development, and that in this context as well, reducing the gene dosage of *Rumi* enhances the function of JAG1.

In summary, our data demonstrate that on a C57BL/6 genetic background, *Jag1* heterozygosity results in significant bile duct paucity accompanied by defects in VSMC recruitment and/or differentiation, and suggest that these animals can be used as a model for Alagille syndrome. We also provide evidence that the protein *O*-glucosyltransferase Rumi glycosylates JAG1 and opposes its function in the liver, potentially by regulating its level and/or cleavage. Additional studies are required to determine the precise role of Rumi in the regulation of JAG1 activity.

Supplementary Material

Refer to Web version on PubMed Central for supplementary material.

Acknowledgments

We thank Dr. Thomas Gridley (Maine Medical Center Research Institute) for generously providing the *Jag1*^{dDSL} mutant strain, Dr. Eva Zsigmond and Mr. Aleksey Domozhirov (Institute of Molecular Medicine, UT-Houston) for help with the generation of the *Rumi*^{flox} allele, and Mr. Edgar Gonzalez for technical assistance.

Financial Support

Supported in part by Cell Lineage and Differentiation Research Grant No. 1-FY10-501 and the Basil O'Connor Starter Award No. 5-FY07-654 from the March of Dimes Foundation (H.J.-N.), and R01GM084135 (H.J.-N.) and R01GM061126 (R.S.H.) from the NIH.

List of Abbreviations

αSMA	alpha smooth muscle actin
BEC	biliary epithelial cell
CK	cytokeratin
EGF repeat	epidermal growth factor-like repeat
H&E	Hematoxylin and Eosin
IHBD	intrahepatic bile duct
Jag1	mouse jagged1 gene
JAG1	jagged1 protein
VSMC	vascular smooth muscle cell
ws-CK	wide spectrum cytokeratin
WT	wild-type

References

1. Kopan R, Ilagan MX. The canonical Notch signaling pathway: unfolding the activation mechanism. Cell. 2009; 137:216–233. [PubMed: 19379690]
2. Lozier J, McCright B, Gridley T. Notch signaling regulates bile duct morphogenesis in mice. PLoS ONE. 2008; 3:e1851. [PubMed: 18365007]
3. Hofmann JJ, Zovein AC, Koh H, Radtke F, Weinmaster G, Iruela-Arispe ML. Jagged1 in the portal vein mesenchyme regulates intrahepatic bile duct development: insights into Alagille syndrome. Development. 2010; 137:4061–4072. [PubMed: 21062863]
4. High FA, Lu MM, Pear WS, Loomes KM, Kaestner KH, Epstein JA. Endothelial expression of the Notch ligand Jagged1 is required for vascular smooth muscle development. Proc Natl Acad Sci U S A. 2008; 105:1955–1959. [PubMed: 18245384]
5. Alagille D, Odievre M, Gautier M, Dommergues JP. Hepatic ductular hypoplasia associated with characteristic facies, vertebral malformations, retarded physical, mental, and sexual development, and cardiac murmur. J Pediatr. 1975; 86:63–71. [PubMed: 803282]
6. Li L, Krantz ID, Deng Y, Genin A, Banta AB, Collins CC, et al. Alagille syndrome is caused by mutations in human Jagged1, which encodes a ligand for Notch1. Nature genetics. 1997; 16:243–251. [PubMed: 9207788]

7. Oda T, Elkahloun AG, Pike BL, Okajima K, Krantz ID, Genin A, et al. Mutations in the human Jagged1 gene are responsible for Alagille syndrome. Nature genetics. 1997; 16:235–242. [PubMed: 9207787]
8. Emerick KM, Rand EB, Goldmuntz E, Krantz ID, Spinner NB, Piccoli DA. Features of Alagille syndrome in 92 patients: frequency and relation to prognosis. Hepatology (Baltimore, Md. 1999; 29:822–829.
9. Lykavieris P, Hadchouel M, Chardot C, Bernard O. Outcome of liver disease in children with Alagille syndrome: a study of 163 patients. Gut. 2001; 49:431–435. [PubMed: 11511567]
10. Fortini ME. Notch signaling: the core pathway and its posttranslational regulation. Dev Cell. 2009; 16:633–647. [PubMed: 19460341]
11. Struhl G, Adachi A. Nuclear access and action of notch in vivo. Cell. 1998; 93:649–660. [PubMed: 9604939]
12. Schweisguth F. Notch signaling activity. Curr Biol. 2004; 14:R129–R138. [PubMed: 14986688]
13. Takeuchi H, Haltiwanger RS. Significance of glycosylation in Notch signaling. Biochemical and biophysical research communications. 2014; 453:235–242. [PubMed: 24909690]
14. Acar M, Jafar-Nejad H, Takeuchi H, Rajan A, Ibrani D, Rana NA, et al. Rumi is a CAP10 domain glycosyltransferase that modifies Notch and is required for Notch signaling. Cell. 2008; 132:247–258. [PubMed: 18243100]
15. Fernandez-Valdivia R, Takeuchi H, Samarghandi A, Lopez M, Leonardi J, Haltiwanger RS, et al. Regulation of the mammalian Notch signaling and embryonic development by the protein O-glucosyltransferase Rumi. Development. 2011; 138:1925–1934. [PubMed: 21490058]
16. McCright B, Lozier J, Gridley T. A mouse model of Alagille syndrome: Notch2 as a genetic modifier of Jag1 haploinsufficiency. Development. 2002; 129:1075–1082. [PubMed: 11861489]
17. Xue Y, Gao X, Lindsell CE, Norton CR, Chang B, Hicks C, et al. Embryonic lethality and vascular defects in mice lacking the Notch ligand Jagged1. Hum Mol Genet. 1999; 8:723–730. [PubMed: 10196361]
18. Fernandez-Valdivia R, Jeong J, Mukherjee A, Soyal SM, Li J, Ying Y, et al. A mouse model to dissect progesterone signaling in the female reproductive tract and mammary gland. Genesis. 2010; 48:106–113. [PubMed: 20029965]
19. Holtwick R, Gotthardt M, Skryabin B, Steinmetz M, Potthast R, Zetsche B, et al. Smooth muscle-selective deletion of guanylyl cyclase-A prevents the acute but not chronic effects of ANP on blood pressure. Proc Natl Acad Sci U S A. 2002; 99:7142–7147. [PubMed: 11997476]
20. Postic C, Shiota M, Niswender KD, Jetton TL, Chen Y, Moates JM, et al. Dual roles for glucokinase in glucose homeostasis as determined by liver and pancreatic beta cell-specific gene knock-outs using Cre recombinase. J Biol Chem. 1999; 274:305–315. [PubMed: 9867845]
21. Sparks EE, Huppert KA, Brown MA, Washington MK, Huppert SS. Notch signaling regulates formation of the three-dimensional architecture of intrahepatic bile ducts in mice. Hepatology (Baltimore, Md. 2010; 51:1391–1400.
22. Xu A, Haines N, Dlugosz M, Rana NA, Takeuchi H, Haltiwanger RS, et al. In vitro reconstitution of the modulation of Drosophila Notch-ligand binding by Fringe. J Biol Chem. 2007; 282:35153–35162. [PubMed: 17923477]
23. Nita-Lazar A, Haltiwanger RS. Methods for analysis of O-linked modifications on epidermal growth factor-like and thrombospondin type 1 repeats. Methods Enzymol. 2006; 417:93–111. [PubMed: 17132500]
24. Rana NA, Nita-Lazar A, Takeuchi H, Kakuda S, Luther KB, Haltiwanger RS. O-glucose trisaccharide is present at high but variable stoichiometry at multiple sites on mouse Notch1. J Biol Chem. 2011; 286:31623–31637. [PubMed: 21757702]
25. Ryan MJ, Bales C, Nelson A, Gonzalez DM, Underkoffler L, Segalov M, et al. Bile duct proliferation in Jag1/fringe heterozygous mice identifies candidate modifiers of the Alagille syndrome hepatic phenotype. Hepatology (Baltimore, Md. 2008; 48:1989–1997.
26. Gouw AS, Clouston AD, Theise ND. Ductular reactions in human liver: diversity at the interface. Hepatology (Baltimore, Md. 2011; 54:1853–1863.

27. Gu H, Marth JD, Orban PC, Mossmann H, Rajewsky K. Deletion of a DNA polymerase beta gene segment in T cells using cell type-specific gene targeting. Science. 1994; 265:103–106. [PubMed: 8016642]
28. Jafar-Nejad H, Leonardi J, Fernandez-Valdivia R. Role of glycans and glycosyltransferases in the regulation of Notch signaling. Glycobiology. 2010; 20:931–949. [PubMed: 20368670]
29. Spinner NB, Colliton RP, Crosnier C, Krantz ID, Hadchouel M, Meunier-Rotival M. Jagged1 mutations in alagille syndrome. Human mutation. 2001; 17:18–33. [PubMed: 11139239]
30. Warthen DM, Moore EC, Kamath BM, Morrissette JJ, Sanchez P, Piccoli DA, et al. Jagged1 (JAG1) mutations in Alagille syndrome: increasing the mutation detection rate. Human mutation. 2006; 27:436–443. [PubMed: 16575836]
31. Antoniou A, Raynaud P, Cordi S, Zong Y, Tronche F, Stanger BZ, et al. Intrahepatic bile ducts develop according to a new mode of tubulogenesis regulated by the transcription factor SOX9. Gastroenterology. 2009; 136:2325–2333. [PubMed: 19403103]
32. Zong Y, Panikkar A, Xu J, Antoniou A, Raynaud P, Lemaigre F, et al. Notch signaling controls liver development by regulating biliary differentiation. Development. 2009; 136:1727–1739. [PubMed: 19369401]
33. Takeuchi H, Fernandez-Valdivia RC, Caswell DS, Nita-Lazar A, Rana NA, Garner TP, et al. Rumi functions as both a protein O-glucosyltransferase and a protein O-xylosyltransferase. Proc Natl Acad Sci U S A. 2011; 108:16600–16605. [PubMed: 21949356]
34. Leonardi J, Fernandez-Valdivia R, Li YD, Simcox AA, Jafar-Nejad H. Multiple O-glucosylation sites on Notch function as a buffer against temperature-dependent loss of signaling. Development. 2011; 138:3569–3578. [PubMed: 21771811]
35. Perdigoto CN, Schweisguth F, Bardin AJ. Distinct levels of Notch activity for commitment and terminal differentiation of stem cells in the adult fly intestine. Development. 2011; 138:4585–4595. [PubMed: 21965616]
36. Ma W, Du J, Chu Q, Wang Y, Liu L, Song M, et al. hCLP46 regulates U937 cell proliferation via Notch signaling pathway. Biochemical and biophysical research communications. 2011; 408:84–88. [PubMed: 21458412]
37. Geisler F, Nagl F, Mazur PK, Lee M, Zimber-Strobl U, Strobl LJ, et al. Liver-specific inactivation of Notch2, but not Notch1, compromises intrahepatic bile duct development in mice. Hepatology (Baltimore, Md. 2008; 48:607–616.
38. Moloney DJ, Shair LH, Lu FM, Xia J, Locke R, Matta KL, et al. Mammalian Notch1 is modified with two unusual forms of O-linked glycosylation found on epidermal growth factor-like modules. J Biol Chem. 2000; 275:9604–9611. [PubMed: 10734111]
39. Nehring LC, Miyamoto A, Hein PW, Weinmaster G, Shipley JM. The extracellular matrix protein MAGP-2 interacts with Jagged1 and induces its shedding from the cell surface. J Biol Chem. 2005; 280:20349–20355. [PubMed: 15788413]
40. Lu J, Ye X, Fan F, Xia L, Bhattacharya R, Bellister S, et al. Endothelial Cells Promote the Colorectal Cancer Stem Cell Phenotype through a Soluble Form of Jagged-1. Cancer cell. 2013
41. Lee TV, Sethi MK, Leonardi J, Rana NA, Buettner FF, Haltiwanger RS, et al. Negative regulation of notch signaling by xylose. PLoS genetics. 2013; 9:e1003547. [PubMed: 23754965]
42. Raynaud P, Carpentier R, Antoniou A, Lemaigre FP. Biliary differentiation and bile duct morphogenesis in development and disease. Int J Biochem Cell Biol. 2011; 43:245–256. [PubMed: 19735739]
43. Shibuya M. Vascular endothelial growth factor and its receptor system: physiological functions in angiogenesis and pathological roles in various diseases. Journal of biochemistry. 2013; 153:13–19. [PubMed: 23172303]
44. Shim WS, Ho IA, Wong PE. Angiopoietin: a TIE(d) balance in tumor angiogenesis. Molecular cancer research : MCR. 2007; 5:655–665. [PubMed: 17634421]
45. Takeuchi H, Kantharia J, Sethi MK, Bakker H, Haltiwanger RS. Site-specific O-glucosylation of the epidermal growth factor-like (EGF) repeats of notch: efficiency of glycosylation is affected by proper folding and amino acid sequence of individual EGF repeats. J Biol Chem. 2012; 287:33934–33944. [PubMed: 22872643]

46. Benedito R, Roca C, Sorensen I, Adams S, Gossler A, Fruttiger M, et al. The notch ligands Dll4 and Jagged1 have opposing effects on angiogenesis. Cell. 2009; 137:1124–1135. [PubMed: 19524514]

47. Li D, Masiero M, Banham AH, Harris AL. The notch ligand JAGGED1 as a target for anti-tumor therapy. Frontiers in oncology. 2014; 4:254. [PubMed: 25309874]

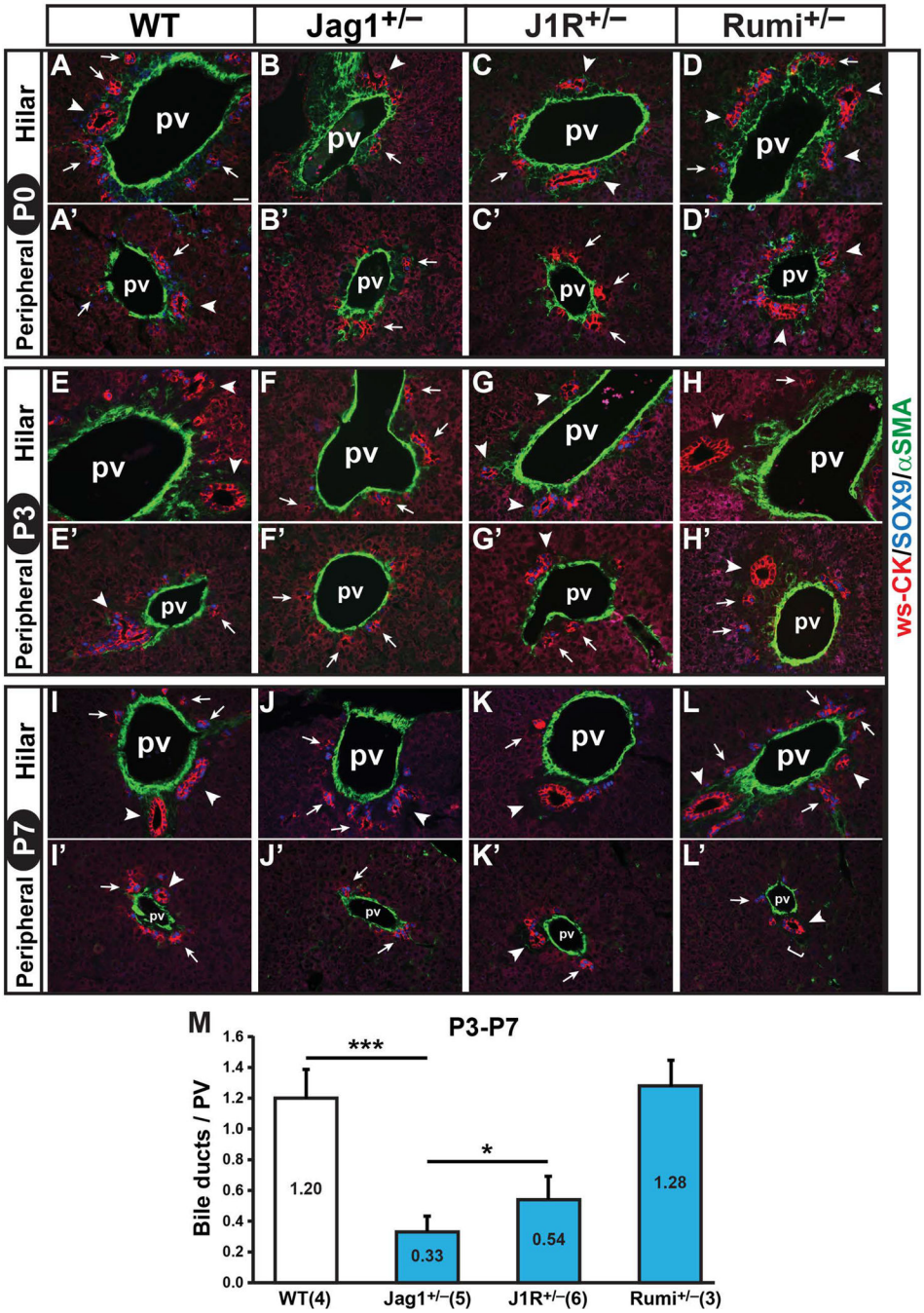

Fig. 1. *Jag1* heterozygous mice show severe impairment of bile duct development during the first postnatal week

(A-L') Liver sections of indicated genotypes and ages stained for αSMA (green), ws-CK (red) and SOX9 (blue). Compared to their WT littermates, *Jag1*$^{+/-}$ livers show weak SOX9 staining and BEC recruitment at P0 (B,B') and P3 (F,F'). Well demarcated bile ducts (indicated by arrowheads) start appearing at P0 in WT (A,A',E,E',I,I') but are hard to identify in *Jag1*$^{+/-}$ livers even at P7 (B,B',F,F',J,J'). *J1R*$^{+/-}$ livers show better bile duct formation in portal veins closer to the hilum at all 3 time points examined (C,G,K) compared

to their *Jag1*$^{+/-}$ littermates (B,F,J). At P0, patent bile ducts (indicated by arrowheads) around peripheral PVs can only be identified in WT and *Rumi*$^{+/-}$ livers (A',D') but not in the other two genotypes (B',C'). At P3 patent bile ducts with surrounding mesenchyme start forming around peripheral PVs of *J1R*$^{+/-}$ livers (G') but are absent in *Jag1*$^{+/-}$ livers (F'). By P7, patent bile ducts can be readily seen around peripheral PVs in *J1R*$^{+/-}$ livers (K'), whereas *Jag1*$^{+/-}$ livers still show a severe paucity of bile ducts in their periphery (J'). (L') Notice the well-defined bile duct with an adjacent faintly αSMA-stained impression of a hepatic artery in a very small peripheral PV of a *Rumi*$^{+/-}$ liver (square bracket). Complete portal triads like this are very common in the periphery of *Rumi*$^{+/-}$ livers, more so than WT. Also note that SOX9 staining is generally weaker in P0 and P3 *Jag1*$^{+/-}$ livers compared to all other genotypes. N ≥ 3 for each genotype at each time point; pv, portal vein; arrowheads indicate bile ducts; arrows indicate foci of ductal plate duplication and remodeling; Scale bar ~25μm. (M) BDs per portal vein were quantified by surveying entire liver sections that were at a similar depth from periphery and labeled with CK. Shown here are the combined counts from P3 and P7 livers. The number of mice analyzed for each genotype is in adjacent brackets (horizontal axis title). Bars represent mean ± S.E.M. ***P<0.005, *P<0.05.

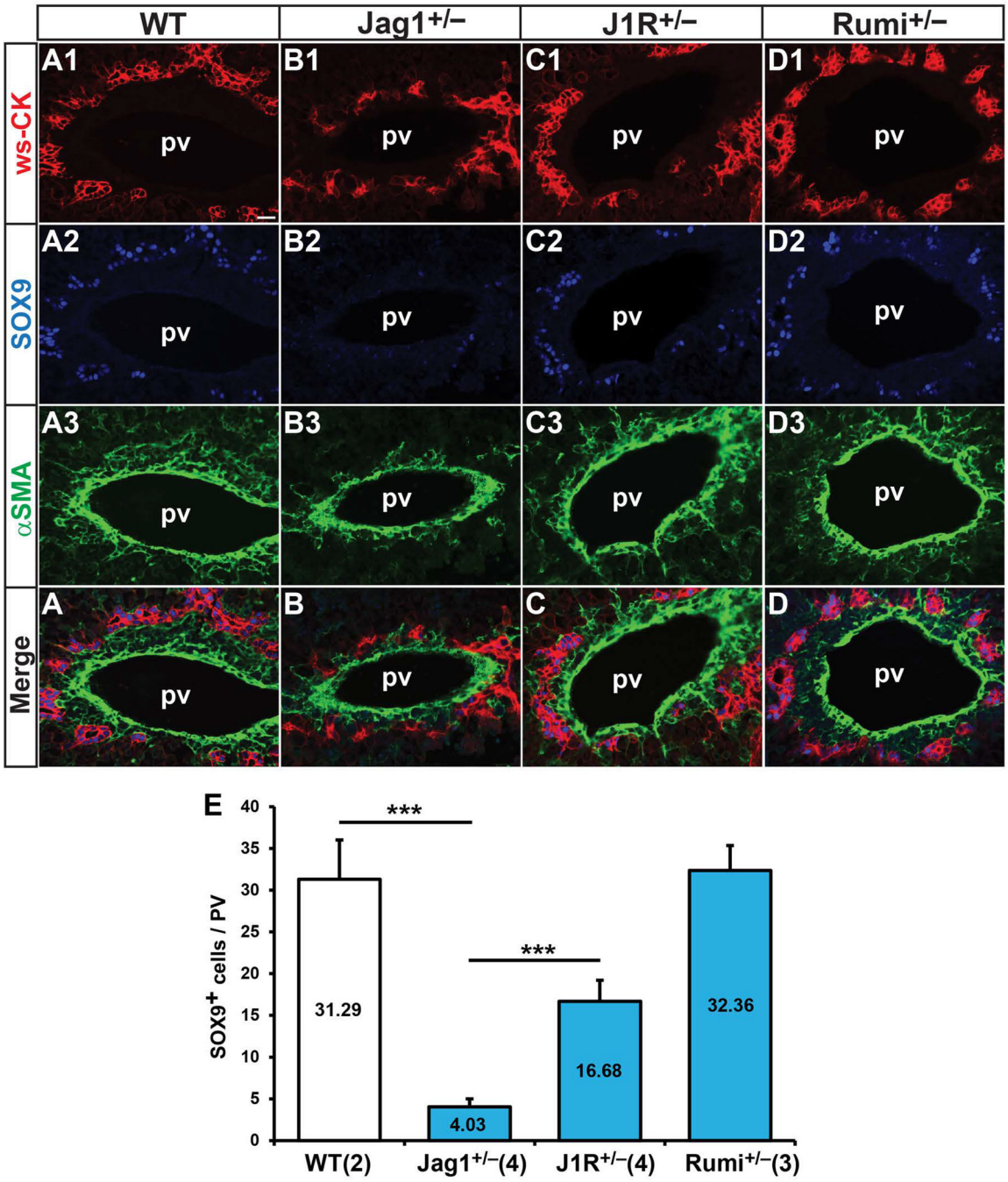

Fig. 2. Improved BEC and VSMC recruitment around embryonic portal veins of *J1R*$^{+/-}$ mice

(A1-D) Paraffin sections of livers harvested from E18 litters were immunostained with ws-CK, SOX9 and αSMA. Each color channel is shown separately, with the merged image in the lowermost panels. Ductal plate in *Jag1*$^{+/-}$ livers is sparse and appears disorganized (B1) compared to WT (A1), *J1R*$^{+/-}$ (C1) and *Rumi*$^{+/-}$ (D1). SOX9 staining is almost absent in E18 *Jag1*$^{+/-}$ livers (B2) but significantly improved in *J1R*$^{+/-}$ livers (C2). αSMA staining appears to be confined to the endothelial vicinity in *Jag1*$^{+/-}$ PVs (B3, compare to A3,C3,D3), evident also by the close proximity of the ductal plate to the vascular

endothelium (B, compare to A,C,D). pv, portal vein; Scale bar ~25μm. (E) Quantification of SOX9 positive cells around the PVs of each liver. All PVs in the whole liver section were counted. The number of mice analyzed for each genotype is in adjacent brackets (horizontal axis title). Bars represent mean ± S.E.M. ***$P<0.005$.

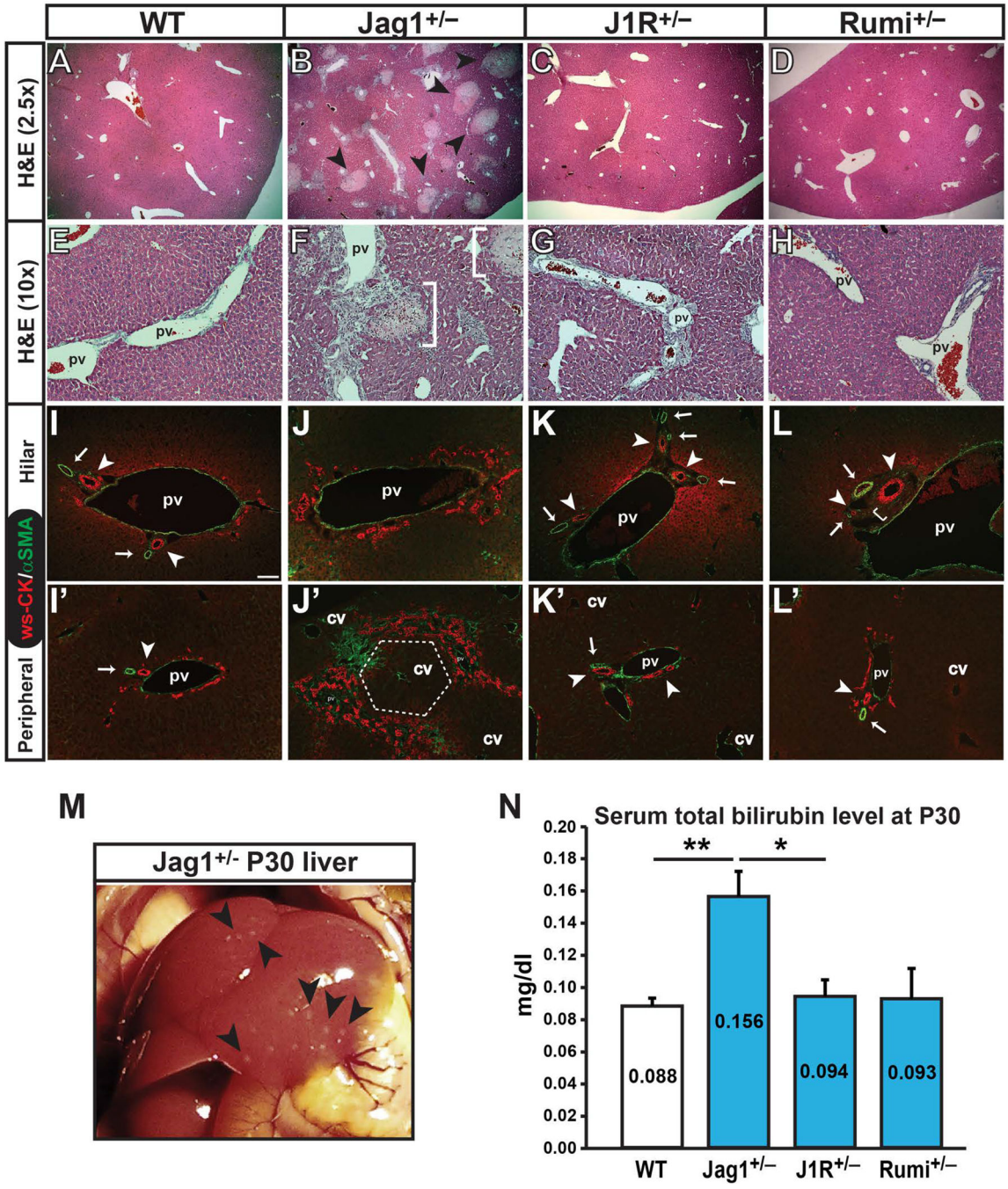

Fig. 3. *Jag1*$^{+/-}$ mice present with widespread ductular reactions at P30 which are suppressed in their *J1R*$^{+/-}$ littermates

(A-L') P30 *Jag1*$^{+/-}$ livers show ductular reactions with bile duct proliferation and inflammatory cell infiltrates (F), sometimes involving up to 60–70% of portal veins in whole liver sections. There are also frequent focal necrotic lesions (arrowheads in B and square brackets in F). Often times the ductular reaction traces the entire margin of a hepatic lobule (J', dotted line). *J1R*$^{+/-}$ littermate livers resemble their WT counterparts at low magnification (C) and have comparatively mild reactions in a few portal triads (G).

Immunostained *J1R*$^{+/-}$ liver sections show normal development of BDs and HAs in most portal triads (K, arrowheads and arrows). (L) *Rumi*$^{+/-}$ livers frequently show thickening of the arterial smooth muscle layer (arrows) and BD epithelium (arrowheads). Also note the prominent peri-ductal mesenchyme (square brackets) frequently observed in *Rumi*$^{+/-}$ livers. pv, portal vein; cv, central vein; arrowheads indicate bile ducts; arrows indicate hepatic arteries; I–L' scale bar ~80μm. (M) Focal necroinflammatory lesions (arrowheads) were visible on the intact livers of 5 out of 11 P30 *Jag1*$^{+/-}$ mice analyzed. (N) Serum analysis for total bilirubin at P30 shows a small but significant elevation of total bilirubin in *Jag1*$^{+/-}$ mice. N=5 for all genotypes except *Rumi*$^{+/-}$ N=4; Bars represent mean ± S.E.M. $^{**}P<0.01$, $^{*}P<0.05$.

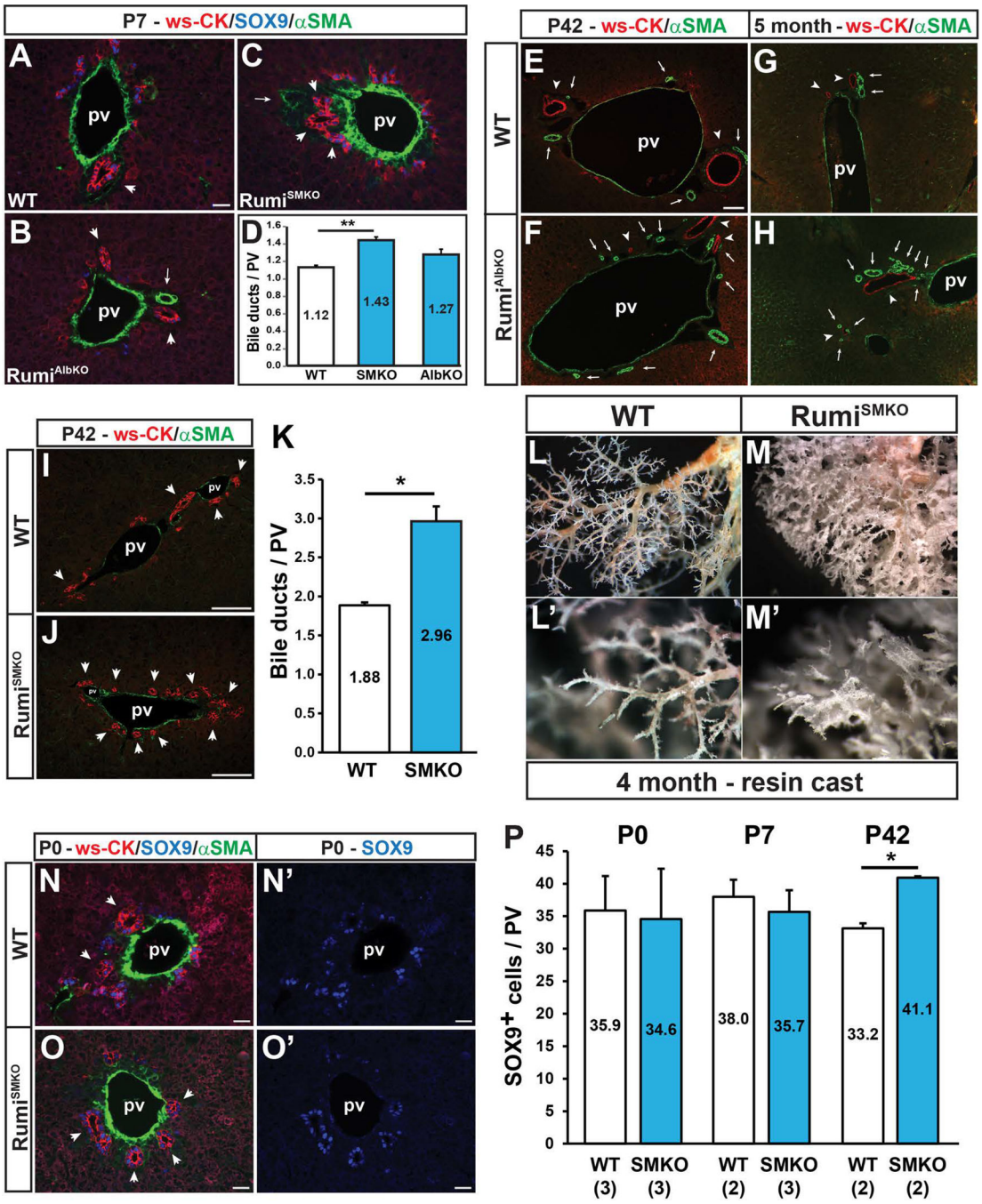

Fig. 4. Targeted deletion of *Rumi* in the SM22α-lineage results in excessive terminal branching of the biliary tree

(A–D) Examination of P7 livers for bile duct abnormalities shows that deletion of *Rumi* in the albumin-positive cell lineages (*Rumi*^{AlbKO}) does not result in any changes in bile duct quantity or morphology (B and D), whereas *Rumi*^{SMKO} mice show an increase in bile ducts per portal vein ratio at this stage (C and D). (B) Note the well-defined, strongly αSMA-positive hepatic artery (arrow) visible in *Rumi*^{AlbKO} portal tracts. N ≥ 3 for each genotype; Scale bar ~25μm. For D, N= WT (4), *Rumi*^{SMKO} (3), *Rumi*^{AlbKO} (2); Bars represent mean ±

S.E.M. **P<0.01. (E–H) *Rumi*^{AlbKO} mice at P42 and 5 months show no bile duct abnormalities in their livers, but an increased number of hepatic arteries is seen in a number of portal triads (arrows). N = 2 for each genotype at each time point; Scale bar ~80μm. (I–K) P42 *Rumi*^{SMKO} livers also show a significantly larger number of BDs in their portal tracts (arrowheads in J, compare to I). N=2. Scale bar ~80μm. Bars represent mean ± S.E.M. *P<0.05. (L-M') 3D resin casts of the biliary tree performed in 4-month-old *Rumi*^{SMKO} mice and their WT littermates support the histological observations of excessive IHBD arborization. N = 3 for each genotype. (N-O') At P0, *Rumi*^{SMKO} livers show more efficient bile duct formation even around smaller PVs (O, compare to N). (N',O') SOX9 staining pattern is comparable between WT and *Rumi*^{SMKO} livers. N ≥ 3 for each time point; Scale bar ~25μm. (P) WT and *Rumi*^{SMKO} mice show a similar number of SOX9^{+} BECs around PVs at P0 and P7. However, at P42, *Rumi*^{SMKO} mice show a small but significant increase in the number of SOX9^{+} BECs around PVs compared to WT littermates. The number of mice analyzed for each genotype is in adjacent brackets (horizontal axis title). *P<0.05.

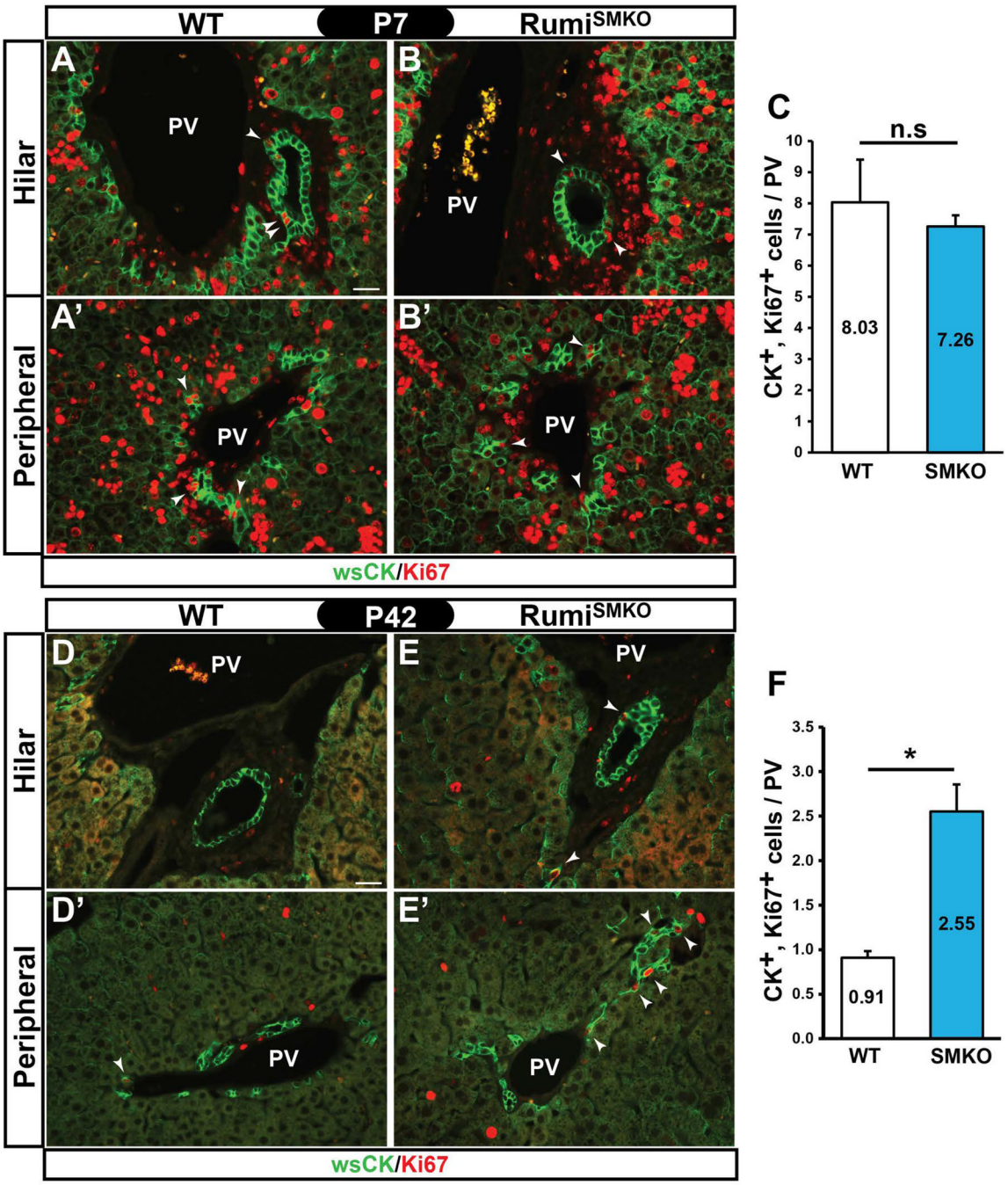

Fig. 5. Targeted deletion of *Rumi* in the SM22α-lineage leads to an increase in the number of proliferating BECs by 6 weeks of age

(A-B',C) At P7, WT and *Rumi*^{SMKO} livers do not show a statistically significant difference in the number of CK$^+$ BECs that are in a state of proliferation as indicated by the expression of Ki67 (arrowheads). N=2. Scale bar ~25μm. Bars represent mean ± S.E.M. (D-E',F) In contrast, at P42 a significantly larger number of CK$^+$ BECs are found to be proliferating (arrowheads), especially around PVs farther from the hilum. N=2. Scale bar ~25μm. Bars represent mean ± S.E.M. **P*<0.05.

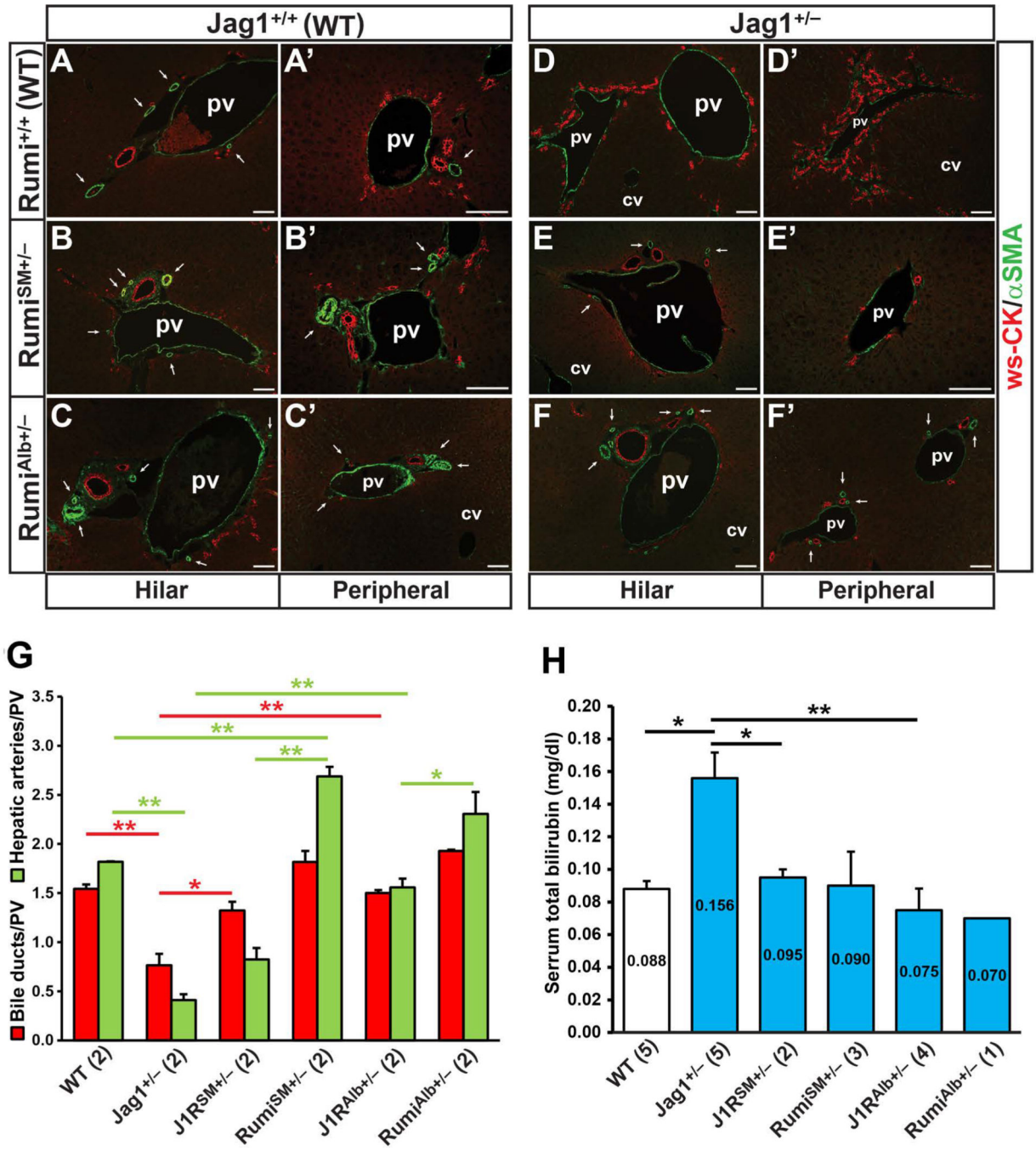

Fig. 6. Reduction of Rumi with either *Albumin-Cre* or *SM22α-Cre* partially rescues the bile duct impairment in *Jag1*$^{+/-}$ livers

Shown are immunofluorescent staining of P30 liver sections from indicated genotypes with antibodies against αSMA (green) and ws-CK (red) with similar staining protocols and exposure times. (A,A') Wild-type PVs showing the entire complement of BD and HAs. (D,D') *Jag1*$^{+/-}$ PVs mostly lack well-defined BDs, and αSMA^{+} HA branches are rarely present. At P30 both *J1*$^{+/-}$*R*$^{SM+/-}$ mice (E,E') and *J1*$^{+/-}$*R*$^{Alb+/-}$ (F,F') show better bile duct and portal triad formation than *Jag1*$^{+/-}$ alone. Note that the rescue in *J1*$^{+/-}$*R*$^{Alb+/-}$ livers

extends farther into the periphery than $J1^{+/-}R^{SM+/-}$ livers (F', compare to E'). Also note the increased number of HA branches frequently observed in the portal triads of $Rumi^{SM+/-}$ (B,B') and $Rumi^{Alb+/-}$ (C,C') livers, a phenomenon which is suppressed by concomitant reduction of *Jag1* (E-F'). N ≥ 2 for each genotype; arrows indicate HA branches; Scale bar ~80μm. (G) Quantification of patent bile ducts and hepatic arteries in P30 livers shown in A–F'. Removing one copy of *Rumi* with *SM22α-Cre* restores the BD/PV ratio in $Jag1^{+/-}$ livers and removing one copy of *Rumi* with *Albumin-Cre* restores both BD/PV and HA/PV ratios in $Jag1^{+/-}$ livers. Note that the apparent increase in the HA/PV ratio in $Rumi^{Alb+/-}$ livers compared to WT livers did not reach statistical significance. However, removing one copy of *Jag1* significantly decreased the HA/PV ratio in $Rumi^{Alb+/-}$ animals. Statistical analysis for significance was done using one-way ANOVA. N=2. Bars represent mean ± S.E.M. **P*<0.05, ***P*<0.01. (H) Serum analysis for total bilirubin at P30 shows a return to WT levels in both $J1^{+/-}R^{SM+/-}$ ($J1R^{SM+/-}$) and $J1^{+/-}R^{Alb+/-}$ ($J1R^{Alb+/-}$) mice. The WT and $Jag1^{+/-}$ values are the same values shown in Fig 3N. The number of mice analyzed for each genotype is in adjacent brackets (horizontal axis title). Statistical analysis for significance was done using one-way ANOVA. Bars represent mean ± S.E.M. **P*<0.05, ***P*<0.01.

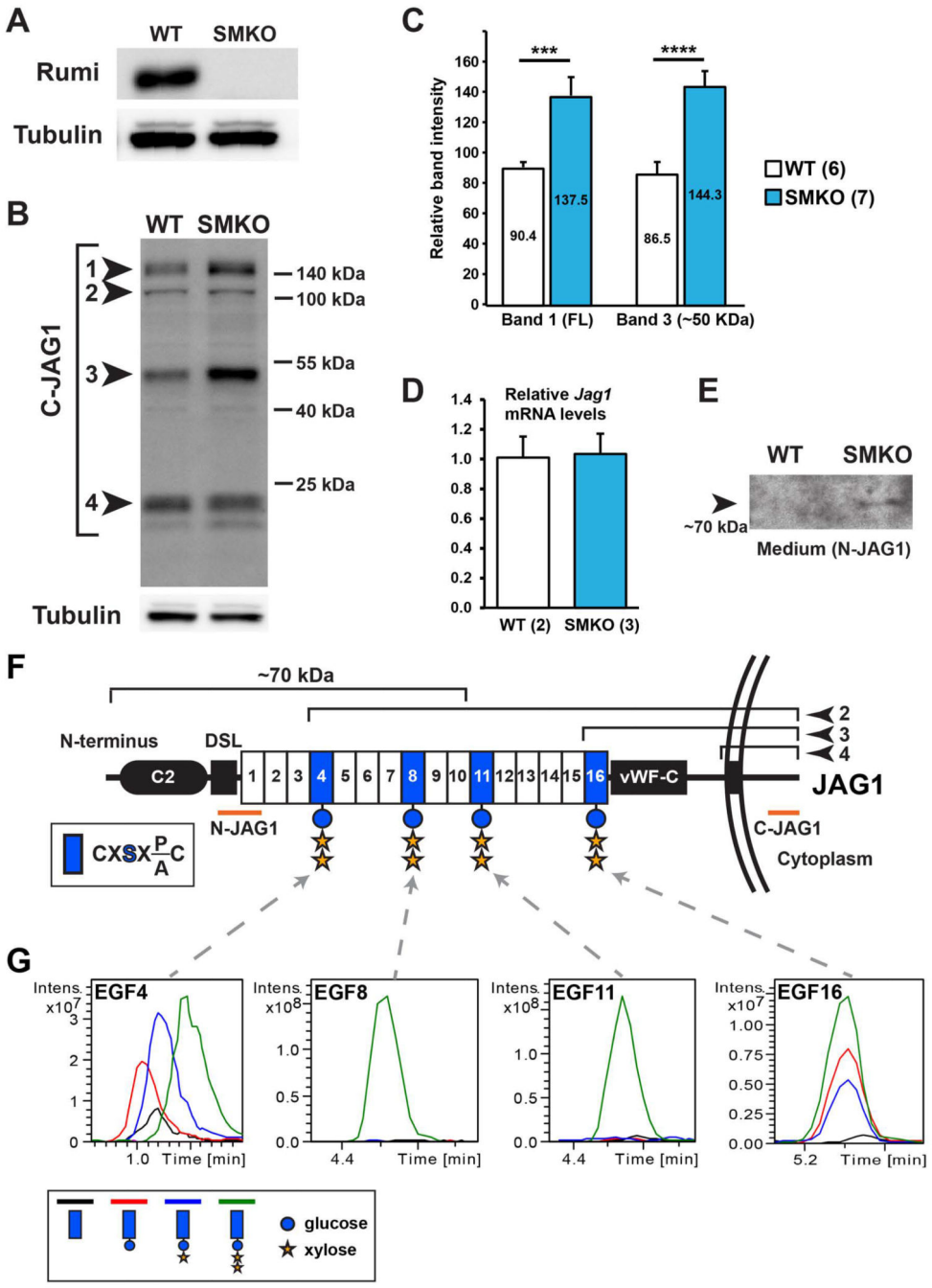

Fig. 7. Deletion of Rumi in VSMCs alters JAG1 protein levels in these cells, and human JAG1 is efficiently *O*-glucosylated

(A–C) VSMCs harvested from inferior vena cavae of WT or *Rumi*^{SMKO} (SMKO) mice were grown to confluence in 6-well plates, trypsinized and lysed for immunoblot analysis. (A) The ~46 kDa Rumi band was not detected in SMKO lysates, indicating that Rumi is efficiently deleted from *Rumi*^{SMKO} VSMCs. (B) Western blotting with anti-C-JAG1 antibody shows four prominent bands labeled 1–4. Band 1 corresponds to the predicted size of full-length JAG1 (~150 kDa). Note that bands 1 and 3 are increased in *Rumi*^{SMKO}

VSMCs. Membrane was stripped and reprobed with anti-α-tubulin as loading control (lower panel). A representative blot from Western blots on VSMCs isolated from 6 independent WT, and 7 *Rumi*^{SMKO} animals is shown. (C) Quantification of band intensities using α-tubulin as loading control shows ~52% increase in FL JAG1 (band 1 and ~67% increase in the ~50 kDa fragment in *Rumi*^{SMKO} VSMCs compared to WT. N= 6 (WT), 7 (SMKO). Bars represent mean ± S.E.M. ***P<0.005, ****P<0.0005. (D) qRT-PCR assay shows no difference in *Jag1* mRNA levels between WT and *Rumi*^{SMKO} VSMCs. N= 2 (WT), 3 (SMKO). Bars represent mean ± S.E.M. (E) Immunoblot analysis of conditioned media from WT and *Rumi*^{SMKO} VSMC cultures with anti-N-JAG1. Note that even when only 10,000 cells are cultured, a soluble form of JAG1 is detected in *Rumi*^{SMKO} but not in WT VSMC conditioned media. A representative blot from two independent experiments is shown. (F) Diagrammatic sketch of mouse/human JAG1 molecule. DSL (Delta-Serrate-Lag2) is part of the Notch binding domain of the ligand. Boxes 1–16 represent EGF repeats in JAG1 ECD. EGF4, 8, 11 and 16 (blue) contain the Rumi target sequence CXSX(P/A)C. Brackets marked 2, 3 and 4 represent an approximation of the corresponding bands in (B). Note the correlation between the location of Rumi target sites and the size of JAG1 fragments detected in Western blots. vWF-C, von Willebrand factor type C domain; C2, phospholipid recognition domain; N-JAG1, approximate epitope location of JAG1 anti-N-terminal Ab; C-JAG1, approximate epitope location of JAG1 anti-C-terminal Ab. (G) Extracted Ion Chromatogram data from mass spectral analysis of EGF4, EGF8, EGF11 and EGF16 from human JAG1. All four predicted Rumi target sites are efficiently *O*-glucosylated. EGF8 and EGF11 only show the fully extended, trisaccharide modification, but EGF4 and EGF16 show all four possibilities (naked EGF, monosaccharide, disaccharide and trisaccharides). Still, the naked EGF (black line) is the least prevalent form of these EGF repeats. EGF16 is also modified by an *O*-fucose residue, which is not shown here for simplicity (please see Supporting Fig. S5). Full spectra and the peptide sequences are shown in Supporting Figure S5.

Table 1

Mendelian analysis and body weights of mice with *Jagged1* and *Rumi* mutations

Cross	Progeny Genotype	Total Mice	Observed %	Expected %
Jag1$^{+/-}$ × WT	WT	199	66	50
(progeny n=304)	*Jag1*$^{+/-}$	105	34	50
			***	
Jag1$^{+/-}$ × *Rumi*$^{+/-}$	WT	45	28	25
(progeny n=160)	*Jag1*$^{+/-}$	26	16	25
	J1R$^{+/-}$	36	23	25
	Rumi$^{+/-}$	53	33	25
			*	

Genotype	Body Weight (g) at P30
WT	16.29 ± 1.02
Jag1$^{+/-}$	12.67 ± 0.56
	**
J1R$^{+/-}$	14.89 ± 1.19
Rumi$^{+/-}$	16.36 ± 1.01

The number of *Jag1*$^{+/-}$ progeny was nearly half of their WT siblings. χ^2 test;

***<0.001. A similar difference between *Jag1*$^{+/-}$ and WT counts was observed in progeny of *Jag1*$^{+/-}$ × *Rumi*$^{+/-}$ crosses, whereas *J1R*$^{+/-}$ counts approach the expected ratio. χ^2 test;

* $P<0.05$. A similar pattern was noticed with the body weights of these animals, with $Jag1^{+/-}$ mice showing significant growth retardation compared to WT, and $J1R^{+/-}$ mice trending towards WT weights.

** $P<0.01$ with unpaired *t*-test (n=7 for all four genotypes)